Uğur Türkan, Mustafa Güden* and Mert Sudağıdan

Staphylococcus epidermidis adhesion on surface-treated open-cell Ti6Al4V foams

DOI 10.1515/bmt-2015-0007
Received January 16, 2015; accepted May 7, 2015; online first June 9, 2015

Abstract: The effect of alkali and nitric acid surface treatments on the adhesion of *Staphylococcus epidermidis* to the surface of 60% porous open-cell Ti6Al4V foam was investigated. The resultant surface roughness of foam particles was determined from the ground flat surfaces of thin foam specimens. Alkali treatment formed a porous, rough $Na_2Ti_5O_{11}$ surface layer on Ti6Al4V particles, while nitric acid treatment increased the number of undulations on foam flat and particle surfaces, leading to the development of finer surface topographical features. Both surface treatments increased the nanometric-scale surface roughness of particles and the number of bacteria adhering to the surface, while the adhesion was found to be significantly higher in alkali-treated foam sample. The significant increase in the number of bacterial attachment on the alkali-treated sample was attributed to the formation of a highly porous and nanorough $Na_2Ti_5O_{11}$ surface layer.

Keywords: bacterial adhesion; foam; *Staphylococcus epidermidis*; surface roughness; surface treatment.

Introduction

The biocompatible porous form of Ti and Ti6Al4V alloy implants are known to provide enhanced interactions with bone due to the higher degree of bone in-growth and body fluid transport through three-dimensional interconnected arrays of pores, leading to improved implant fixation [24]. In addition, the relatively low elastic moduli of porous implants reduce the extent of stress shielding, causing well-known implant loosening [18]. One potential application of Ti and Ti alloy foams has been identified in spinal surgery as the bone-fixating porous spinal interbody fusion cages [9, 36]. Titanium and Ti6Al4V alloy foams can be prepared by means of a relatively simple process known as the space holder method [27] with typical pore sizes of 200–500 μm and porosities up to 80% [45]. Furthermore, calcium phosphate (CaP) coatings on porous surfaces including Ti mesh [39, 41] and sintered powder (beads) compacts [22, 32] were shown to have beneficial effects on bone-generating properties, improving implant fixation to bone. Bone-like apatite coating on Ti essentially enhances the surface osteoblast cell adhesion and differentiation [11] and increases the bone bonding strength by allowing an early bone opposition to implant [47]. Basically, Ti metals have limited bioactivity due to their extremely thin passive oxide layer [12]. Previously, biomimetic CaP coating on porous Ti was shown to be very effective in developing a continuous and homogeneous coating layer. Various surface treatments were also applied to increase the bioactivity of Ti metal in conjunction with biomimetic CaP coating.

An effective way of increasing the bioactivity of Ti metal is to modify the surfaces with NaOH and HNO_3 at elevated temperatures. Kim et al. [14] showed that alkali surface treatment and subsequent heat treatment improved the bioactivity of Ti. When Ti metal is immersed in alkali solution, the surface passive TiO_2 layer is partially dissolved due to the aggressive environment containing hydroxyl groups. This produces negatively charged hydrates, $HTiO_3^- \cdot nH_2O$, then reacts with positively charged alkali ions in aqueous solution, resulting in a porous thin sodium titanate gel layer on the surface of Ti [14, 15, 17, 44]. It was recently shown that nitric acid treatment (NAT) in fact increased the surface energy of Ti implants by not significantly affecting the surface roughness [19, 20]. A homogeneous CaP coating layer formed only after 6 days of simulated body fluid (SBF) immersion in an alkali-treated 40% porous sintered Ti powder compact [48]. A recent study showed a very thin layer of CaP formation on Ti6Al4V foams after alkali treatment (AT) and NAT [40].

***Corresponding author: Mustafa Güden,** İzmir Institute of Technology, Department of Mechanical Engineering Center for Materials Research, Gulbahce Koyu, Urla, 35430 Izmir, Turkey, Phone: +90 (232) 7506779, Fax: +90 (232) 7506701, E-mail: mustafaguden@iyte.edu.tr
Uğur Türkan: Department of Biomedical Engineering, Gediz University, Seyrekköy, Menemen, Izmir, Turkey
Mert Sudağıdan: Konya Food and Agriculture University, Meram, Konya, Turkey

The increased use of prosthesis implants has raised an important problem of bacterial infection [8, 30]. The most effective approach to minimizing bacterial infections and their adhesion on implant surfaces involves chemically modifying the biomaterial surface. In this perspective, two facile approaches are of interest in applications. The former approach involves using materials that contain bactericidal substances capable of being incorporated into or bound to the biomaterial surfaces. The latter one is to modify the substrate with the antiadhesive materials to prevent the adhesion of bacteria [7]. A recent study showed that the surface treatment applied to Ti, including sandblasting, micro-arc oxidation, and SBF CaP coating promoted bacterial colonization *in vitro*, which was mainly attributed to the increased surface roughness, hence the increased surface area with the applied surface treatment [42]. There are essentially numerous studies and few review articles in the literature reporting the increased tendency of bacterial colonization with increasing surface roughness [1, 16, 26, 37, 42]. The bacterial colonization on Ti6Al4V alloy was reported to occur preferentially in vanadium-rich regions [10], while surface nitriding and berberine inhibited the bacterial adhesion to Ti6Al4V surfaces [28, 43]. Despite the experimental studies on bacterial adhesion to bulk Ti6Al4V alloy surfaces, there has been no investigation on the bacterial colonization of Ti6Al4V alloy foams, a group of materials that have been widely investigated for biomedical applications in the last decade [5, 6, 9, 23, 27, 33–36]. The aim of the present study is, therefore, to investigate the effect of the most widely used NAT and AT on *Staphylococcus epidermidis* adhesion to an open-cell Ti6Al4V foam. Staphylococci are one of the most common pathogens found in implant-related infections [49, 50]; for this reason, it was used in this study. The bacterial colonization is considered important as the foam samples are soaked into SBF solution for a relatively long period. To assess the effect of surface roughness on bacterial adhesion, the roughness of the ground flat surfaces of foam particles was measured in nanometric scale before and after surface treatment.

Materials and methods

An open-cell Ti6Al4V alloy foam with ~60% porosity was prepared through a space holder method using ammonium bicarbonate (Aldrich, St. Louis, MO, USA) as space holder. The chemical composition of the used gas atomized spherical Ti6Al4V powder (Crucible Research, Pittsburgh, PA, USA) complied with the ASTM 1580-1 standard [3]. The particle size of the Ti6Al4V powder ranged from 45 to 150 μm, with an average size of 94 μm. Figure 1A and B shows the SEM image of Ti6Al4V particles and particle size distribution, respectively. Nearly 80% of particles are >60 μm, showing a monomodal particle size distribution (Figure 1B). The details of Ti6Al4V foam preparation, the microstructure development after sintering, and the mechanical properties of prepared foams are given elsewhere [9]. Briefly, the green powder compacts

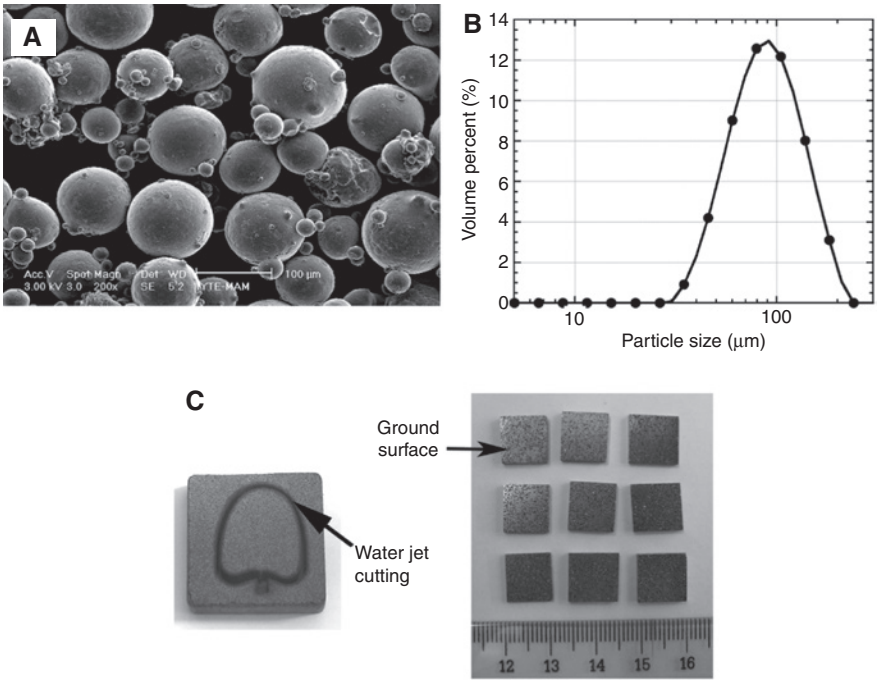

Figure 1: (A) SEM micrographs of Ti6Al4V particles; (B) particle size distributions of powder; and (C) water jet cut foam sample plate and microbial foam test specimens.

uniaxially pressed at 200 MPa were heat treated at 200°C for 2 h to remove the space holder; then, the compact was sintered at 1300°C for 1 h under a high-purity (99.998%) Ar flux. The foams prepared with the above-mentioned method showed ~60% porosity. Figure 1C shows a picture of a water jet-cut sintered foam plate and small square cross-section plate-like bacterial adhesion foam test specimens (10×10×3 mm^3) cut from sintered foam plates using a low-speed diamond saw. The foam specimens' square cross-sections were then ground sequentially down to 2400 grit SiC paper. Therefore, the foam specimens' surfaces are composed of ground flat regions and inner cells (pores). After grinding, the foam specimens were cleaned ultrasonically in acetone, then in ethyl alcohol, and finally in deionized water for 15 min. NAT was performed in a 1:1 volume ratio solution of HNO_3 (65%) and H_2O at 60°C for 5 h. AT was performed in a 100 ml 10 M NaOH aqueous solution at 60°C for 24 h. Following the surface treatments, the specimens were cleaned ultrasonically in deionized water for 15 min. Nitric acid-treated specimens were dried in air, while alkali-treated specimens were dried in an oven at 40°C for 24 h. The foam samples without surface treatment were also prepared and tested for comparison.

The crystal structure of the powder and surface-treated/untreated foam specimens before the bacterial adhesion test was determined using a Philips Xpert X-ray diffractometer with a Cu-Kα x-ray (λ=1.5404 for 8.05 keV) in grazing incidence (GIXRD) mode at an incident angle of ω=0.5°. The effective depth (sin ω/μ) probed by Cu-Kα was calculated as 174 nm. Microscopic analyses of the samples were performed using a Philips XL30-SFEG scanning electron microscope (SEM). The surface topography, surface roughness (Ra), and surface area difference (SAD) of the foam specimens before and after the surface treatment were determined using a Nanoscope-IV atomic force microscope (AFM) using taping tips (Vecco otespa) with the spring constant of 20–100 N m^{-1}. The scanned area was selected to be 1.5×1.5 μm, with vertical and lateral resolutions of 0.001 and 2 nm, respectively. At least three AFM surface scans were conducted on the randomly selected areas of foam specimen ground flat surfaces and were used to calculate the average surface roughness values.

Biofilm-forming *S. epidermidis* strain YT-169a was grown overnight on tryptic soy agar (TSA) plates at 37°C. The bacterial suspension was prepared in sterile 0.9% (w/v) NaCl and adjusted to McFarland 1.0 (3×10^8 cells ml^{-1}). One hundred microliters of bacterial suspension was inoculated to 10 ml tryptic soy broth supplemented with 1% (w/v) sucrose-containing foam specimens in six-well culture plates. The specimens with bacteria were incubated at 37°C for 24 h with shaking at 60 rpm. Following the incubation, the specimens were washed three times with sterile phosphate-buffered saline (PBS) in order to remove non-adherent bacteria and then transferred into 25 ml PBS. The adherent bacteria were removed from the foam specimens under sonication (15 min) and using sterile cell scrapers. The removed bacteria from surfaces were serially diluted to 10^{-4} and 10^{-5} with PBS, and 100 μl of the diluted bacteria were spread onto duplicate TSA plates. The plates were incubated at 37°C for 24 h, and the number of *S. epidermidis* colonies were counted and quantified as colony-forming units per milliliter (CFU ml^{-1}). At least three samples were used herein, and the results were presented as mean±standard deviation.

Results

Figure 2 shows the GIXRD spectra of untreated and alkali- and nitric acid-treated Ti6Al4V foam particles. Although

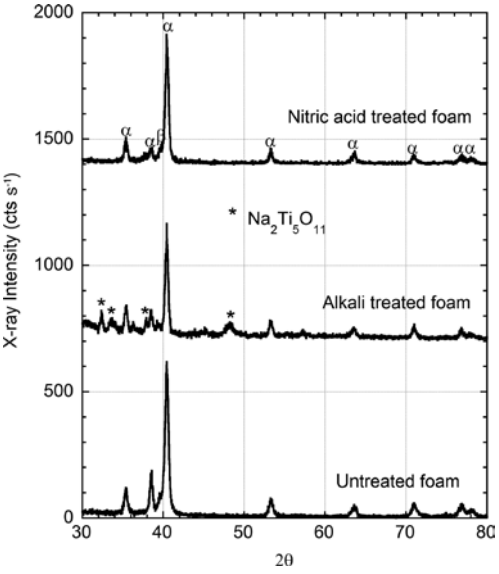

Figure 2: GIXRD pattern of untreated, nitric acid-treated and alkali-treated foam samples.

the microstructure of as-received powders was composed of a needle-like α phase, referred as acicular α, sintering at 1300°C transformed the needle-like α into Widmanstätten structure of β lathes (bcc and rich in V) and α platelets (hcp and rich in Al), as seen in Figure 2. As marked with "*" in Figure 2, AT forms a thin layer of $Na_2Ti_5O_{11}$ on Ti6Al4V particles.

The untreated foam cellular structure depicted in Figure 3A shows bimodal pore size distributions: macropores (300–500 μm) and micropores (1–30 μm). Micropores resulted from the space in between the sintered Ti6Al4V particles on the cell walls and at the cell edges (marked by arrows in Figure 3A), while macropores resulted from the space holder removal. The thickness of $Na_2Ti_5O_{11}$ layer is about 500 nm, measured from the SEM picture shown in the inset of Figure 3B. It is also noted in the same micrographs that porous $Na_2Ti_5O_{11}$ layer accommodates microcracks. Figure 4A shows an AFM micrograph (1.5×1.5 $μm^2$) of the untreated foam flat surface. A major grinding line passing along the mid-section is clearly seen in this figure. Figure 4B,C shows sequentially the AFM micrographs of nitric acid- and alkali-treated foam flat surfaces. NAT essentially increases the number of nanometric-scale undulations on the foam flat surfaces, leading to the development of finer surface topographical features (Figure 4B), while AT forms a rougher surface topography (Figure 4C) as compared with untreated and nitric acid-treated foam surfaces (Figure 4A). The measured Ra and SAD values of untreated and surface-treated foams are listed in Table 1. Both NAT and AT increase the foam specimen flat surface roughness in nanometric scale, while the increase is higher

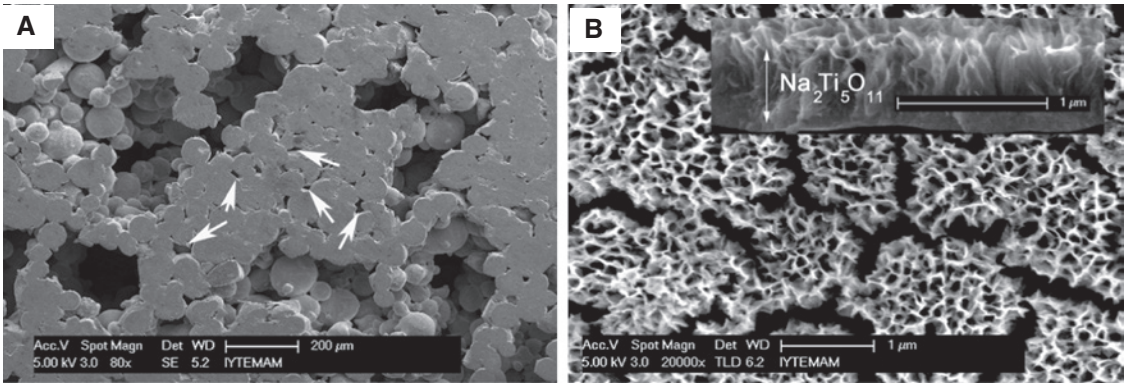

Figure 3: SEM micrographs of (A) foam surfaces, showing micropores on the cell walls and (B) alkali-treated foam flat surfaces, showing a porous surface layer.

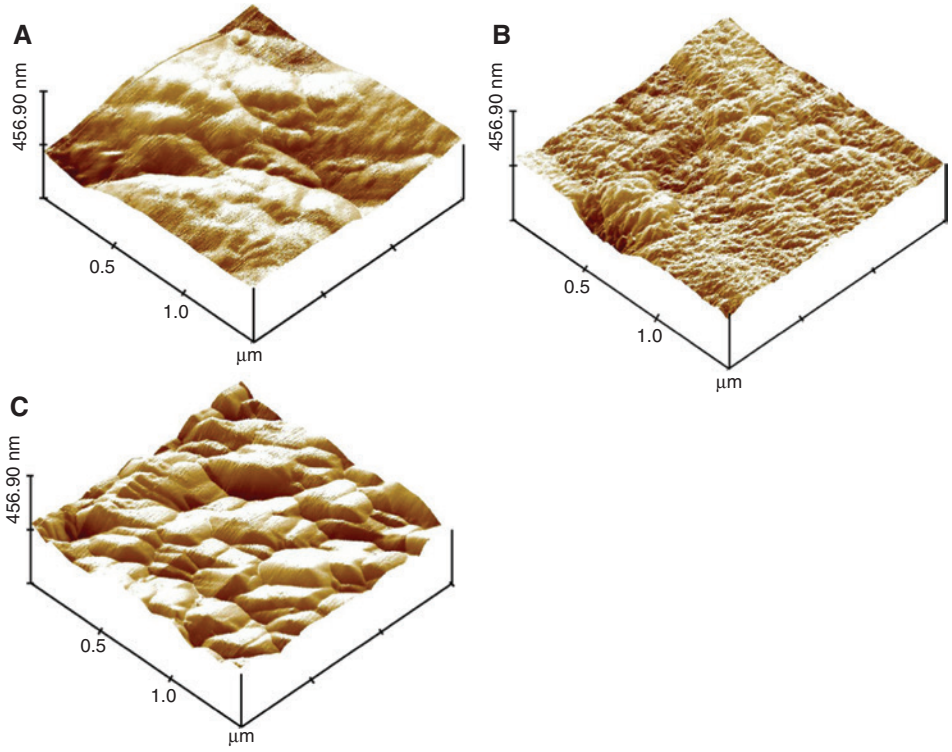

Figure 4: Three-dimensional AFM micrographs of the surface topography of (A) untreated, (B) nitric acid-treated, and (C) alkali-treated foam specimen.

Table 1: Surface roughness of foam flat surfaces before the microbial test.

Treatment	Ra (nm)	SAD (%)
Untreated	10.715	1.279
NAT	12.012	3.832
AT	15.769	5.477

in the alkali-treated foam sample. The surface treatment essentially causes significant increase in the surface area, resulting from finer surface microstructure development.

Microscopically higher numbers of bacterial colonization are detected on the flat surfaces and interior of the cells of the surface-treated foams, as seen in Figure 5A–C. It is also noted that the preferential bacterial colonization

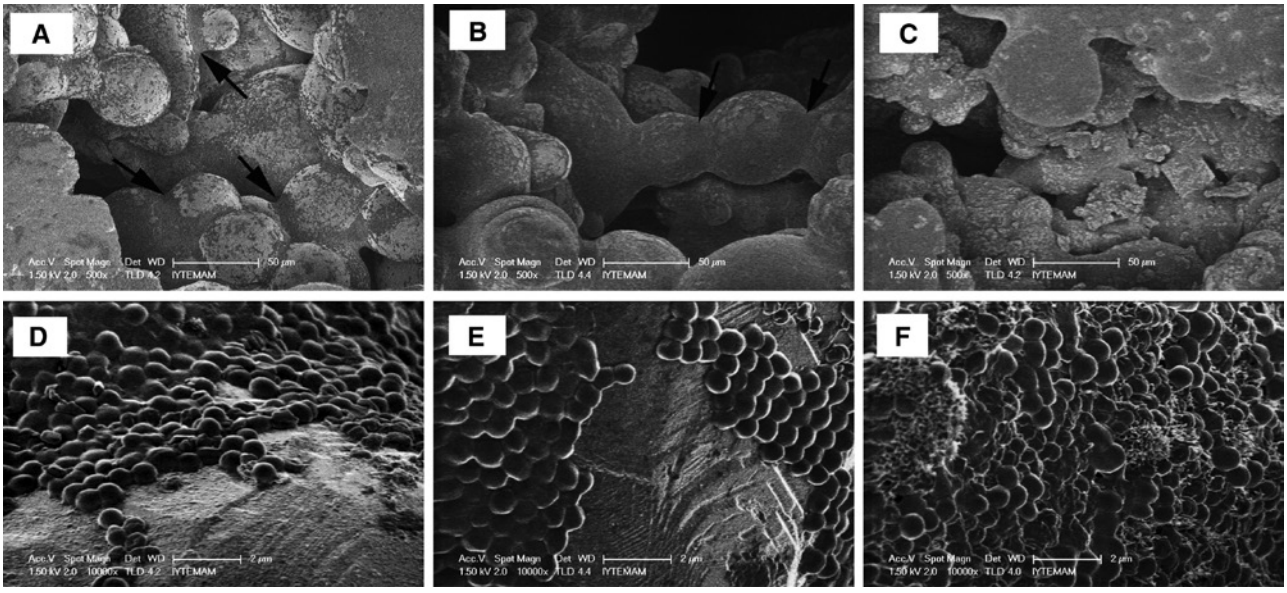

Figure 5: SEM micrographs of *S. epidermidis* bacteria attached to interior of cells in (A) untreated, (B) nitric acid-treated, and (C) alkali-treated foams, and SEM micrographs of *S. epidermidis* bacteria on Ti6Al4V particles in (D) untreated, (E) nitric acid-treated, and (F) alkali-treated foams.

occurs at the particle sintering necks marked with arrows in Figure 5A,B. The magnified SEM micrographs of Ti6Al4V particles of untreated and nitric acid- and alkali-treated foams are sequentially shown in Figure 5D–F. The fully bacteria-covered particle surface of the alkali-treated sample seen in Figure 5F also confirms higher bacterial adhesion to alkali-treated foam sample surfaces. Figure 6A shows the number of bacteria attached to the surface of untreated and treated foam specimens. As seen in the same graph, the surface treatment increases the number of bacteria attached to the foam surface over that of untreated foam specimen: the bacterial adhesion is tripled in nitric acid-treated foam, while the number of bacteria retained increases eight times in alkali-treated foam. In order to analyze the effect of nanometric-scale surface roughness on the bacterial colonization, CFU values of the investigated untreated and treated foam specimens are drawn as function of nanometric-scale surface roughness values in Figure 6B. As seen in Figure 6B, a linear interpolation to log CFU vs. roughness data shows that the CFU values of foams increase with increasing roughness of foam flat surfaces.

Discussion

The factors influencing the bacterial adhesion to a solid surface and the interactions between bacteria and

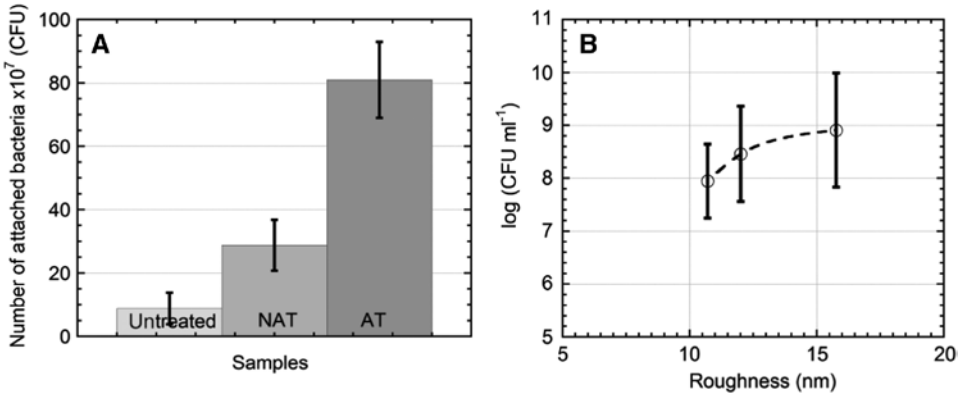

Figure 6: (A) Attached bacteria (CFU) and (B) CFU vs. surface roughness of untreated and treated foam specimens.

nanometer surface topologies were reviewed in different studies [1, 2, 4]. Broadly, these included the characteristics of bacteria, target surface, and the environment [1]. In an earlier study, no significant effect of surface roughness on *S. epidermidis* adhesion to Ti surface was reported for the surface roughness values of 0.44 and 1.25 μm [27]. The effects of nanometric-scale surface topographical features on *Staphylococcus aureus* and *Pseudomonas aeruginosa* adhesion to Ti surface have recently been experimentally investigated [25]. Four different surface topologies were explored: conventional, nanorough, nanotubular, and nanotextured. The results clearly indicated that nanometric surface topologies affected the bacterial adhesion. Nanometric-scale surface topographical features both increased the surface energy and altered the surface chemistry. Although conventional and nanorough Ti surfaces had the same surface chemistry, the increased surface area of nanorough Ti surface resulted in intensified fibronection adsorption, leading to reduced bacterial adhesion. The effect of nanometric-scale surface roughness on bacterial adhesion to an ultrafine crystalline (equal channel angular processed) Ti was also investigated [38]. The polished surface roughness of conventional and ultrafine crystalline Ti samples measured using AFM at different scanning areas increased in nanometric scale with increasing scanning area. Ultrafine crystalline Ti samples with higher nanoroughness showed two times higher *S. aureus* adhesion than conventional Ti samples. Similar effects of nanoscale surface topologies on protein adsorption to polymer surfaces were also reported previously [13, 46]. It is generally accepted that bacteria preferentially attach to rougher surfaces. A rough surface provides a larger surface area for bacterial adhesion and protects the bacteria form shear forces [29]. Bacterial colonization also occurs more preferentially on porous (foam) than smooth surfaces [21]. AT forms a porous and rough thin surface layer of sodium titanate on Ti metal [14, 15, 17, 44]. The morphology of this layer is altered with the surface treatment conditions and the applied heat treatment [44].

In the determination of the number of adhered *S. epidermidis* cells, the cells on the materials' surface were removed by sonication after washing non-adherent bacteria and then the remaining cells were scraped off by using sterile cell scrapers. By this way, almost all bacteria from the surface could be detached into the PBS solution. After serial dilution with PBS, they were inoculated onto TSA plates, and after growing at 37°C, the number of colonies were counted and expressed as CFU ml^{-1}. The present results indicate that both NAT and AT increase the bacterial adhesion to Ti6Al4V foam surfaces. The increased bacterial adhesion on alkali-treated foam samples compared to untreated foam samples is attributed to the formation of a highly porous and nanorough $Na_2Ti_5O_{11}$ surface layer and increased nanometric-scale surface roughness. Porous and nanorough $Na_2Ti_5O_{11}$ surface layer increases the surface area, protecting the bacteria from shear forces. Previously, it was reported that NAT did not increase the surface roughness of Ti significantly [20, 31], while it increased the surface energy [19]. The results of the present study, however, also show that NAT increases the nanometric-scale surface roughness of Ti6Al4V foam. The increased bacterial adhesion on nitric acid-treated foam samples compared to untreated foam samples may be partly due to the increased nanometric-scale surface roughness.

The results of the present study, however, should be taken cautiously as the surface roughness of the particles in the interior of the cells cannot be measured directly using AFM. Therefore, the resultant surface roughness of the particles after surface treatment was determined indirectly by measuring the roughness of the foam specimen's ground flat surfaces. The SEM micrographs of the flat surfaces of untreated and treated foam samples are shown in Figure 7A–C. The major grinding lines at a distance of ~5 μm are clearly seen in Figure 7A,B in between the major grinding lines; the minor grinding lines are also detected in the same micrographs. The major grinding lines agree with the AFM surface topography shown in Figure 4A. NAT tends to remove minor grinding lines from the flat surface of foam, as seen in Figure 7B; however, it introduces small undulations on the surface, which is also detected in AFM surface topography image in Figure 4B. The surface morphology of alkali-treated foam specimens is, however, dictated by the nature of $Na_2Ti_5O_{11}$ layer as depicted in Figure 7C. The microcracks seen in the same figure are spaced at a distance of 3–5 μm. The particles in the interior of the cells of untreated foam contain thermal etch facets on the surface (Figure 7D). The heights of the thermal etch facets were further measured using the SEM micrographs of the particles. Thermal etch facet heights varied with the locations of particles' surfaces; therefore, at least 15 measurements were taken randomly from the selected particles, and the results were averaged. The thermal etch facet height was found to be 211 nm for untreated foam particles (Figure 7E). NAT has almost no effect on the thermal etch facet heights – 217 nm (Figure 7E). The development of nanosurface roughness following NAT are clearly seen on the thermal etch facets (Figure 7E). The sodium titanate layer resulting from AT completely covers the thermal etch facets on the particle surfaces, as shown in Figure 7F. The roughness measurements taken from the foam specimen's flat surfaces reflect the surface roughness of the particles

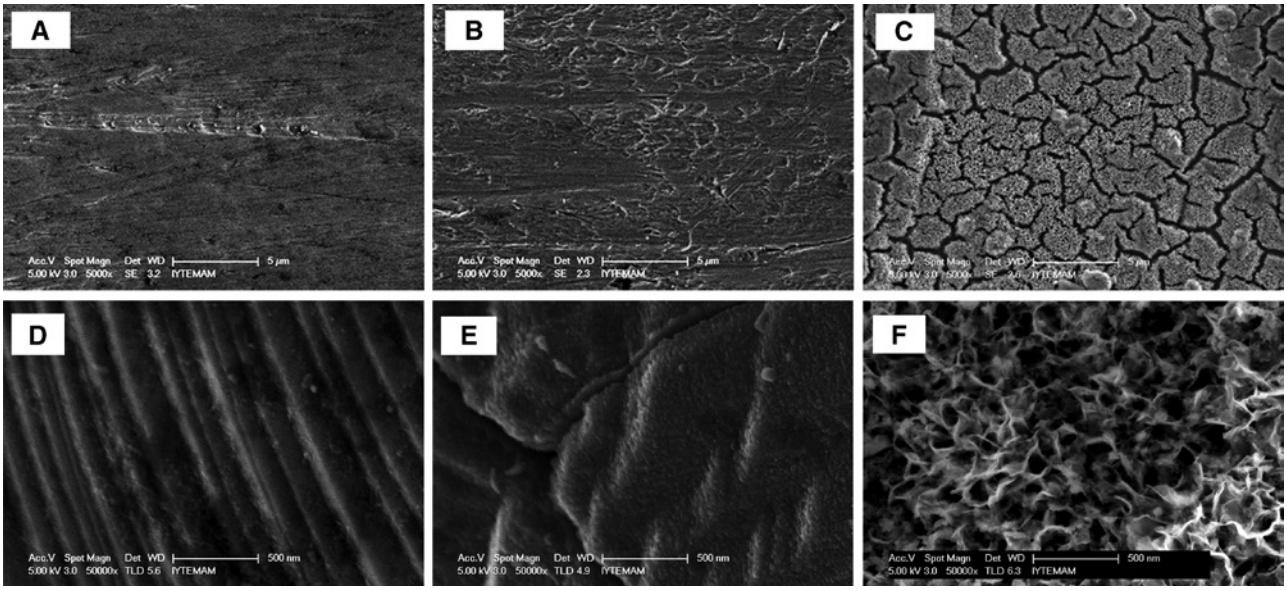

Figure 7: SEM micrographs of the foam flat surfaces of (A) untreated, (B) nitric acid-treated, and (C) alkali-treated, and SEM micrographs of the surface of particles in the interior of cells of (D) untreated, (E) nitric acid-treated, and (F) alkali-treated foams.

in the interior of the cells. An effort to correlate the surface roughness resulting from thermal etch facets with the bacterial colonization essentially shows a decreasing number of bacterial retention with increasing thermal etch facet heights.

Conclusions

The effect of alkali and nitric acid surface treatments on *S. epidermidis* adhesion to the surface of a porous open-cell Ti6Al4V foam (pore sizes of 300–500 μm), prepared by the space holder method using 94 μm average particle size powder, was investigated. The roughness of the ground flat surfaces of the relatively thin foam specimens was measured before and after the surface treatment in nanometric scale using an AFM. AT increased the nanometric-scale surface roughness significantly by developing a porous, rough $Na_2Ti_5O_{11}$ surface layer on the Ti6Al4V particles, while NAT resulted in the formation of finer surface topographical features. In accordance with the surface roughness measurements, the highest number of bacterial retention was detected in the alkali-treated foam specimen, followed by the nitric acid-treated foam sample. A correlation between the nanometric-scale surface roughness and the associated bacterial adhesion was shown. The significant increase in the number of bacterial adhesion on alkali-treated samples was attributed to the formation of a highly porous and nanorough $Na_2Ti_5O_{11}$ surface layer.

References

[1] An YH, Friedman RJ. Concise review of mechanisms of bacterial adhesion to biomaterial surfaces. J Biomed Mater Res 1998; 43: 338–348.
[2] Anselme K, Davidson P, Popa AM, Giazzon M, Liley M, Ploux L. The interaction of cells and bacteria with surfaces structured at the nanometre scale. Acta Biomater 2010; 6: 3824–3846.
[3] ASTM F 1580-95. Standard specification for titanium and Ti6Al4V alloy powders for coating surgical implants.
[4] Bazaka K, Crawford RJ, Ivanova EP. Do bacteria differentiate between degrees of nanoscale surface roughness? Biotechnol J 2011; 6: 1103–1114.
[5] Chen XB, Li YC, Hodgson PD, Wen C. The importance of particle size in porous titanium and nonporous counterparts for surface energy and its impact on apatite formation. Acta Biomater 2009; 5: 2290–2302.
[6] Cheung S, Gauthier M, Lefebvre LP, Dunbar M, Filiaggi M. Fibroblastic interactions with high-porosity Ti-6Al-4V metal foam. J Biomed Mater Res B Appl Biomater 2007; 82B: 440–449.
[7] Chua P-H, Neoh KG, Kang ET, Wang W. Surface functionalization of titanium with hyaluronic acid/chitosan polyelectrolyte multilayers and RGD for promoting osteoblast functions and inhibiting bacterial adhesion. Biomaterials 2008; 29: 1412–1421.
[8] Darouiche RO. Current concepts – treatment of infections associated with surgical implants. N Engl J Med 2004; 350: 1422–1429.
[9] Dizlek ME, Guden M, Turkan U, Tasdemirci A. Processing and compression testing of Ti6Al4V foams for biomedical applications. J Mater Sci 2009; 44: 1512–1519.
[10] Gabriel BL, Gold J, Gristina AG, et al. Site-specific adhesion of *Staphylococcus-epidermidis* (RP12) in Ti-Al-V metal systems. Biomaterials 1994; 15: 628–634.

[11] Gil FJ, Padrós A, Manero JM, Aparicio C, Nilsson M, Planell JA. Growth of bioactive surfaces on titanium and its alloys for orthopaedic and dental implants. Mater Sci Eng C Biomimet Supramol Syst 2002; 22: 53–60.
[12] Grigal IP, Markeev AM, Gudkova SA, Chernikova AG, Mityaev AS, Alekhin AP. Correlation between bioactivity and structural properties of titanium dioxide coatings grown by atomic layer deposition. Appl Surf Sci 2012; 258: 3415–3419.
[13] Khang D, Kim SY, Liu-Snyder P, Palmore GT, Durbin SM, Webster TJ. Enhanced fibronectin adsorption on carbon nanotube/poly(carbonate) urethane: independent role of surface nano-roughness and associated surface energy. Biomaterials 2007; 28: 4756–4768.
[14] Kim HM, Miyaji F, Kokubo T, Nakamura T. Preparation of bioactive Ti and its alloys via simple chemical surface treatment. J Biomed Mater Res 1996; 32: 409–417.
[15] Kokubo T. Development of bioactive materials based on surface chemistry. J Eur Ceram Soc 2008; 29: 1267–1274.
[16] Lan G, Li M, Tan Y, et al. Promoting bone mesenchymal stem cells and inhibiting bacterial adhesion of acid-etched nanostructured titanium by ultraviolet functionalization. J Mater Sci Technol 2015; 31: 182–190.
[17] Lee BH. Surface modification by alkali and heat treatments in titanium alloys. J Biomed Mater Res 2002; 61: 466–473.
[18] Long M, Rack HJ. Titanium alloys in total joint replacement – a materials science perspective. Biomaterials 1998; 19: 1621–1639.
[19] Lu X, Wang Y, Yang X, et al. Spectroscopic analysis of titanium surface functional groups under various surface modification and their behaviors *in vitro* and *in vivo*. J Biomed Mater Res A 2008; 84A: 523–534.
[20] Lu X, Zhao ZF, Leng Y. Biomimetic calcium phosphate coatings on nitric-acid-treated titanium surfaces. Mater Sci Eng C Biomimet Supramol Syst 2007; 27: 700–708.
[21] Merritt K, Shafer JW, Brown SA. Implant site infection rates with porous and dense materials. J Biomed Mater Res 1979; 13: 101–108.
[22] Nguyen HQ, Deporter DA, Pilliar RM, Valiquette N, Yakubovich R. The effect of sol-gel-formed calcium phosphate coatings on bone ingrowth and osteoconductivity of porous-surfaced Ti alloy implants. Biomaterials 2004; 25: 865–876.
[23] Oh IH, Simon V, Vida-Simiti I, Batin G, Candea V, Simon S. Mechanical properties of porous titanium compacts prepared by powder sintering. Scr Mater 2003; 49: 1197–1202.
[24] Pilliar RM. Porous-surfaced metallic implants for orthopedic applications. J Biomed Mater Res Appl Biomater 1987; 21: 1–33.
[25] Puckett SD, Taylor E, Raimondo T, Webster TJ. The relationship between the nanostructure of titanium surfaces and bacterial attachment. Biomaterials 2010; 31: 706–713.
[26] Rodríguez-Cano A, Cintas P, Fernández-Calderón MC, et al. Controlled silanization-amination reactions on the Ti6Al4V surface for biomedical applications. Colloids Surf B Biointerf 2013; 106: 248–257.
[27] Ryan G, Pandit A, Apatsidis DP. Fabrication methods of porous metals for use in orthopaedic applications. Biomaterials 2006; 27: 2651–2670.
[28] Sarro MI, Moreno DA, Ranninger C, King E, Ruiz J. Influence of gas nitriding of Ti6Al4V alloy at high temperature on the adhesion of *Staphylococcus aureus*. Surf Coatings Technol 2006; 201: 2807–2812.
[29] Scheuerman TR, Camper AK, Hamilton MA. Effects of substratum topography on bacterial adhesion. J Colloid Interface Sci 1998; 208: 23–33.
[30] Sculco TP. The economic-impact of infected joint arthroplasty. Orthopedics 1995; 18: 871–873.
[31] Sittig C, Textor M, Spencer ND, Wieland M, Vallotton PH. Surface characterization of implant materials cp Ti, Ti-6Al-7Nb and Ti-6Al-4V with different pretreatments. J Mater Sci Mater Med 1999; 10: 35–46.
[32] Tache A, Gan L, Deporter D, Pilliar RM. Effect of surface chemistry on the rate of osseointegration of sintered porous-surfaced Ti-6Al-4V implants. Int J Oral Maxillofac Implants 2004; 19: 19–29.
[33] Takemoto M, Fujibayashi S, Neo M, Suzuki J, Kokubo T, Nakamura T. Mechanical properties and osteoconductivity of porous bioactive titanium. Biomaterials 2005; 26: 6014–6023.
[34] Takemoto M, Fujibayashi S, Matsushita T, Suzuki J, Kokubo T, Nakamura T. Enhanced osteoinductivity of porous titanium implant by sodium removal. Key Eng Mater 2006; 309–311: 1315–1318.
[35] Takemoto M, Fujibayashi S, Neo M, et al. Osteoinductive porous titanium implants: effect of sodium removal by dilute HCl treatment. Biomaterials 2006; 27: 2682–2691.
[36] Takemoto M, Fujibayashi S, Neo M, et al. A porous bioactive titanium implant for spinal interbody fusion: an experimental study using a canine model. J Neurosurg Spine 2007; 7: 435–443.
[37] Teughels W, Van Assche N, Sliepen I, Quirynen M. Effect of material characteristics and/or surface topography on biofilm development. Clin Oral Implants Res 2006; 17: 68–81.
[38] Truong VK, Lapovok R, Estrin YS, et al. The influence of nano-scale surface roughness on bacterial adhesion to ultrafine-grained titanium. Biomaterials 2010; 31: 3674–3683.
[39] Tsukeoka T, Suzuki M, Ohtsuki C, et al. Enhanced fixation of implants by bone ingrowth to titanium fiber mesh: effect of incorporation of hydroxyapatite powder. J Biomed Mater Res B Appl Biomater 2005; 75B: 168–176.
[40] Turkan U, Guden M. The effect of surface treatment on CaP deposition of Ti6Al4V open cell foams in SBF solution. Ceram Int 2010; 36: 1805–1816.
[41] Vehof JWM, Spauwen PHM, Jansen JA. Bone formation in calcium-phosphate-coated titanium mesh. Biomaterials 2000; 21: 2003–2009.
[42] Wang XJ, Wang G, Liang J, Cheng J, Ma W, Zhao Y. *Staphylococcus aureus* adhesion to different implant surface coatings: an *in vitro* study. Surf Coat Technol 2009; 203: 3454–3458.
[43] Wang XQ, Qiu S, Yao X, Tang T, Dai K, Zhu Z. Berberine inhibits *Staphylococcus epidermidis* adhesion and biofilm formation on the surface of titanium alloy. J Orthopaed Res 2009; 27: 1487–1492.
[44] Wei M, Kim HM, Kokubo T, Evans JH. Optimising the bioactivity of alkaline-treated titanium alloy. Mater Sci Eng C Biomimet Supramol Syst 2002; 20: 125–134.
[45] Wen CE, Mabuchi M, Yamada Y, Shimojima K, Chino Y, Asahina T. Processing of biocompatible porous Ti and Mg. Scr Mater 2001; 45: 1147–1153.

[46] Woo KM, Chen VJ, Ma PX. Nano-fibrous scaffolding architecture selectively enhances protein adsorption contributing to cell attachment. J Biomed Mater Res A 2003; 67A: 531–537.
[47] Yan WQ, Nakamura T, Kawanabe K, Nishigochi S, Oka M, Kokubo T. Apatite layer-coated titanium for use as bone bonding implants. Biomaterials 1997; 18: 1185–1190.
[48] Zhang QY, Leng Y, Xin RL. A comparative study of electrochemical deposition and biomimetic deposition of calcium phosphate on porous titanium. Biomaterials 2005; 26: 2857–2865.
[49] Zimmerli W. Prosthetic-joint-associated infections. Best Pract Res Clin Rheumatol 2006; 20: 1045–1063.
[50] Zimmerli W, Trampuz A, Ochsner PE. Current concepts: prosthetic-joint infections. N Engl J Med 2004; 351: 1645–1654.